

# Dynamics of partially thermalized solutions of the Burgers equation\*

Patricio Clark di Leoni<sup>1,2</sup>, Pablo D. Mininni<sup>1</sup>, & Marc E. Brachet<sup>3</sup>

<sup>1</sup>*Departamento de Física, Facultad de Ciencias Exactas y Naturales,  
Universidad de Buenos Aires and IFIBA, CONICET,  
Ciudad Universitaria, 1428 Buenos Aires, Argentina.*

<sup>2</sup>*Department of Physics and INFN, University of Rome “Tor Vergata”,  
Via della Ricerca Scientifica 1, 00133, Rome, Italy.*

<sup>3</sup>*Laboratoire de Physique Statistique, École Normale Supérieure,  
PSL Research University; UPMC Univ Paris 06, Sorbonne Universités; Université Paris Diderot,  
Sorbonne Paris-Cité; CNRS; 24 Rue Lhomond, 75005 Paris, France.*

(Dated: March 13, 2022)

The spectrally truncated, or finite dimensional, versions of several equations of inviscid flows display transient solutions which match their viscous counterparts, but which eventually lead to thermalized states in which energy is in equipartition between all modes. Recent advances in the study of the Burgers equation show that the thermalization process is triggered after the formation of sharp localized structures within the flow called “tygers”. We show that the process of thermalization first takes place in well defined subdomains, before engulfing the whole space. Using spatio-temporal analysis on data from numerical simulations, we study propagation of tygers and find that they move at a well defined mean speed that can be obtained from energy conservation arguments.

## I. INTRODUCTION

The formulation of a proper microscopic theory of turbulence has remained a major challenge in statistical physics [1]. In spite of this, classic Gibbs ensembles have provided significant insights when used to predict the equilibrium of ideal flows in which only a finite number of spatial modes are allowed [2–4]. For the case of the spectrally truncated three-dimensional Euler equation, energy is then equipartitioned between all modes in a thermalized equilibrium state. This results in an energy spectrum that goes like  $\sim k^2$ , which differs greatly from the  $\sim k^{-5/3}$  Kolmogorov spectrum that is in agreement with experiments and observations. The main hurdle is that macroscopic hydrodynamics is essentially dissipative, and so conservative statistical formulations cannot capture its essence.

Nonetheless, statistical equilibria of spectrally truncated systems have played an important role in turbulence theory. The main reason for this is that they give a proxy for the direction of the energy cascade in the forced and dissipative case [3], and they allow identification of attractors in freely decaying dissipative cases [4]. As an example of the former, they have led to the prediction of the inverse energy cascade in two-dimensional turbulence [3], while an example of the latter is magnetohydrodynamics, where the existence of multiple quadratic invariants results in several long-time possible solutions which were identified using statistical equilibria [4].

Recently the interest on Gibbs ensembles in turbulence was renewed, as it was also found that the transient as the ideal truncated system reaches the equilibrium can mimic forced and dissipative systems. It was originally

suggested by Kraichnan and Chen [1] that truncated conservative systems can behave as dissipative when considering only the spatial modes which have not thermalized. The idea behind this is that high wave number thermalized modes can act as an energy sink for the low wave number modes, which will behave as in a normal turbulent flow. This has been put on firm grounds by computing eddy viscosity caused by thermalized modes and confirmed numerically in high resolution simulations of the Euler equation in [5]. In the simulations, energy was initially concentrated at low wave numbers and was let to cascade to larger ones, and a long transient following the previous description was observed before the system reached full thermalization. The results were extended to helical hydrodynamic flows [6], magnetohydrodynamics [7], compressible flows [8], quantum turbulence [9, 10], gyrokinetic plasma systems [11], the dyamo problem [12, 13], and also to study the decay of quasi-geostrophic turbulence [14].

While systems such as the spectrally truncated Euler equation are known to thermalize and to have a viscous-like transient, not much is known about how thermalization begins and evolves, or about how the limit of the truncation wave number going to infinity behaves. The recent discovery of a phenomenon dubbed as “tygers” [15] in studies of the two-dimensional Euler and of the Burgers equations has opened a new path to tackle these problems. The inviscid Burgers equation is a non-linear PDE known to develop shocks, for which energy-preserving truncations do not converge (in a weak sense) to the inviscid limit [16–18], and whose spectrally truncated version thermalizes in finite time [19]. The curious fact is that the first “spurious” effects of thermalization in physical space do not occur near the shock, but away from it. Sharp localized structures, the so-called tygers, are formed. After collapsing, thermalization starts to take place near the location of the tyger, eventually expanding to the whole

\* Postprint version of the manuscript published in Phys. Rev. Fluids **3**, 014603 (2018)

domain. The mechanism behind the formation of a tyger has been identified as a resonant interaction between fluid particles and truncation noise [15]. Further studies [20] have determined the time between the appearance of a tyger and the onset of thermalization, and its scaling with the truncation wave number. Recent studies have linked the appearance of tygers to a period-doubling bifurcation and loss of stability of the truncated wave solutions [21].

The importance of tygers and the thermalization mechanism is multiple. The Burgers equation has been used as a toy model of turbulence which also displays shocks (see, for example, [22, 23] and references therein). As such, the study of tygers gives information on dynamical processes in the system, and on how modes interact non-linearly. They are also important for numerical methods as they develop and increase error in regions in which the flow is initially smooth, and as their control or removal would allow the development of new methods to integrate equations in the inviscid limit. In particular, when studying numerically the blow-up problem in fluid dynamics (i.e., the formation of a singularity in finite time, for references see [24, 25]), attention should be put in discerning between tygers and actual blow-up effects.

The aim of this paper is to study the evolution of thermalization itself, and how the first traces of thermalization end up engulfing the whole domain. We do this via numerical simulation of the one-dimensional Burgers equation at different truncation wave numbers. It is found that the system first partially thermalizes inside different spatial subdomains, defined by the initial positions of the tygers and shocks. The boundary of the thermalized component then propagates as the system reaches equilibrium with a well defined mean velocity. So, while at long times full stochastic behavior is obtained [19], at intermediate times deterministic and stochastic behaviors are mixed.

## II. THE BURGERS EQUATION

The inviscid one-dimensional Burgers equation, in conservation form, reads

$$\frac{\partial u}{\partial t} + \frac{\partial}{\partial x} \left( \frac{1}{2} u^2 \right) = 0, \quad (1)$$

where  $u$  is the velocity field. Under periodic boundary conditions the solutions can be expanded in wave number space in a Fourier series of the form

$$u(x, t) = \sum_{k=-\infty}^{\infty} \hat{u}_k(t) e^{ikx}, \quad (2)$$

where  $\hat{u}_k(t)$  are the coefficients of the expansion. As we are interested in working with the spectrally truncated version of the equations, we define the Galerkin projector

$$P_{k_G}[u(x, t)] = \sum_{|k| \leq k_G} \hat{u}_k(t) e^{ikx}, \quad (3)$$

which is just a low-pass filter that sets all Fourier modes with wave number  $|k| > k_G$  to zero, and where  $k_G$  is the truncation wave number. The spectrally truncated Burgers equation then reads

$$\frac{\partial}{\partial t} P_{k_G}(u) + \frac{1}{2} \frac{\partial}{\partial x} P_{k_G}(u^2) = 0. \quad (4)$$

This equation conserves linear momentum  $\sum u$  and energy  $\sum u^2$ . It is a well known fact that the continuum (untruncated) Eq. (1) produces a shock in finite time. For the truncated Eq. (4) it has been shown that a resonant interaction between the fluid particles and the truncation noise causes the formation of sharp localized structures, the so-called tygers, in regions in which the flow is smooth [15]. After formation, tygers then collapse and give rise to thermalization. The timescale under which the collapse happens scales as  $\sim k_G^{-4/9}$  [20]. Then, for sufficiently long times, the system reaches full thermalization and all its properties can be predicted using the Gibbs canonical ensemble with partition function

$$Z = C_\beta e^{-\beta \sum_{k=1}^{k_G} |\hat{u}_k|^2}, \quad (5)$$

where  $\beta = k_G / \bar{E}$ , and where  $\bar{E}$  is the mean energy of the flow [19]. For details on the formation of the tygers the reader is referred to the studies in [15, 20, 21], and for the thermalized solutions at late times to [19]. In the following we will be concerned with what happens between the triggering of thermalization and until the subsequent statistical equilibrium is reached.

## III. NUMERICAL SIMULATIONS

For the purpose of this study Eq. (4) was solved numerically using a pseudospectral method with the 2/3 rule for dealiasing, which naturally implements the spectral truncation, and which conserves the energy. Time integration was done using a Runge-Kutta method. Different truncation wave numbers were considered, from  $k_G = 341$  to  $k_G = 10922$ . By virtue of the 2/3 rule, the truncation wave number is  $k_G = N/3$  where  $N$  is the spatial resolution. Thus, simulations with spatial resolutions from  $N = 1024$  to  $N = 32768$  grid points were done. All of these simulations performed have essentially the same behavior, and none of the results we now present depend on  $k_G$  (at least for the values of  $k_G$  we considered, the limit of  $k_G$  going to infinity is highly non-trivial). Therefore, all the figures we present in the main text are from a simulation with  $k_G = 5461$  ( $N = 16384$ ). A comparison between the different resolutions is shown in the Appendix.

Two different initial conditions were used; first, a single-mode initial condition

$$u_1(x) = \cos(x), \quad (6)$$

and then an initial condition with two excited modes

$$u_2(x) = \sin(x) + \sin(2x - 0.741), \quad (7)$$

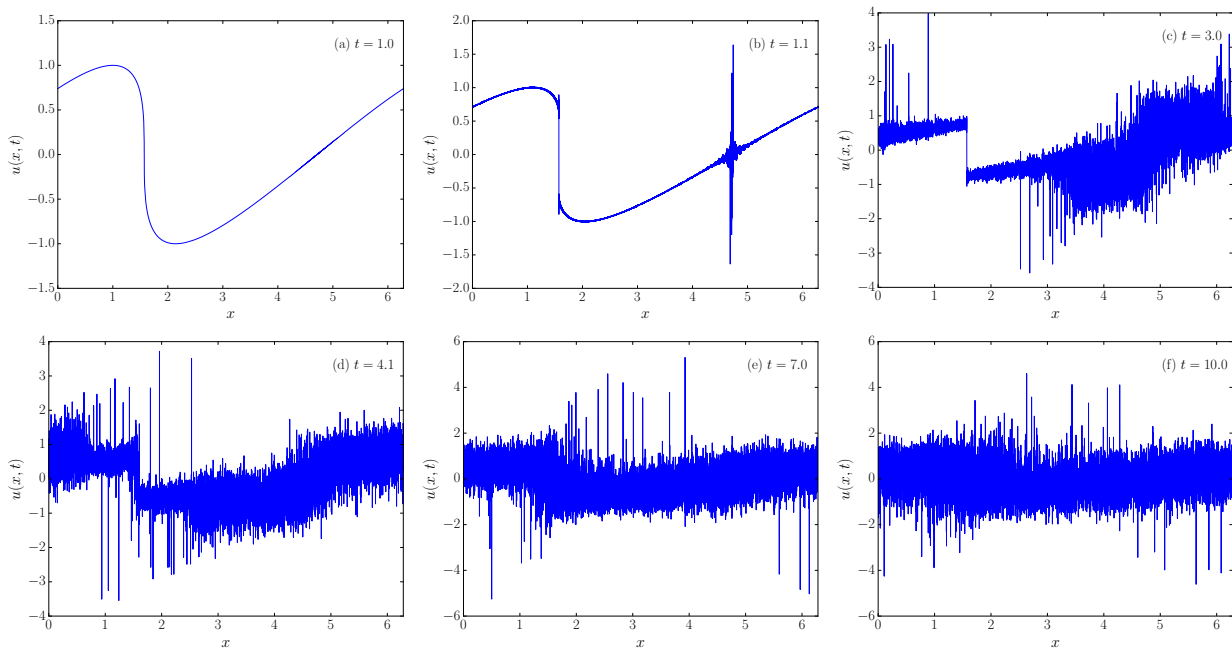


FIG. 1. (Color online) Evolution of  $u(x, t)$  at different times, from (a)  $t = 1$  to (f)  $t = 10$ , in a simulation with  $k_G = 5461$  and a single-mode initial condition given by Eq. (6). The shock is formed at  $t = 1$ , and the tyger has developed and started to collapse at  $t = 1.1$ . Afterwards each front of the tyger advances, swallowing up the rest of the solution. (a)  $t = 1.0$ , (b)  $t = 1.1$ , (c)  $t = 3.0$ , (d)  $t = 4.1$ , (e)  $t = 7.0$ , and (f)  $t = 10.0$ .

which was used before in [15] to study the early time development of tygers.

#### IV. RESULTS

Under the single-mode initial condition  $u_1(x)$  given by Eq. (6), the system develops a shock at  $t = 1$  (see Fig. 1). Snapshots of  $u(x, t)$  at different times, ranging from  $t = 1$  up to  $t = 10$ , are also shown in Fig. 1. At  $t = 1$  only the shock can be seen at  $x = \pi/2$ , while at  $t = 1.1$  the tyger is already present at  $x = 3\pi/2$ . As reported in previous studies [15, 20, 21], the tyger develops in a region in which the velocity is smooth, and its position can be predicted from the fact that it appears at the point of the flow that has positive strain and that travels with the same velocity as the shock (in the case of this simulation,  $u = 0$ ).

At later times in Fig. 1 the tyger collapses and starts to thermalize, seen in the figure as the development of wide regions that look like white noise (although the shock at  $x = \pi/2$  and a linear ramp in the velocity in the rest of the domain can still be recognized at  $t = 3, 4.1$ , and  $7$ ). Note these wide regions propagate to the left and right, respectively with negative and positive velocity. Starting from the tyger, thermalization creeps slowly through space until the whole domain is almost fully thermalized at  $t = 10$ . How these thermalized fronts propagate and what are their statistical properties are the main focuses of this work. From visual inspection, it is easy to see that the velocity of these fronts fluctuates around a cer-

tain value. We will thus study the mean and the variance of these fluctuations (which, as fluctuations are close to Gaussian, are sufficient to characterize their statistical properties). Averaging operations should then be always understood as the spatial average in a certain region of real space, as defined below.

To better understand this evolution we present the spatio-temporal plot of  $u(x, t)$ , and the spatio-temporal energy spectrum in Figures 2(a) and 2(b) respectively. The spatio-temporal evolution of  $u(x, t)$  is similar to those used in the methods of characteristics, to study the formation and evolution of shocks. Indeed, the formation of the shock at  $t = 1$  and at  $x = \pi/2$  is clearly visible as the formation of a sharp horizontal line (note that the shock does not propagate as it has speed  $u = 0$ ). Right after the shock forms, a noisier horizontal line appears at  $x = 3\pi/2$ , with a cone (indicated by two solid lines) that widens linearly with time. This is the tyger and the thermalized region that propagates until covering the entire domain. Remarkably, the propagation of its fronts has clear mean velocities  $U = \pm 2/\pi$ , which is also the slope of the two straight lines in Fig. 2(a).

The spatio-temporal spectrum has been used before to identify structures and waves in turbulent and other complex flows [26, 27]. It is given by

$$E(k, \omega) = |\hat{u}(k, \omega)|^2/2, \quad (8)$$

where  $\hat{u}(k, \omega)$  is the Fourier transform in time of the Fourier coefficients of the velocity  $\hat{u}(k, t)$ . The Fourier transform in time is performed from the moment the

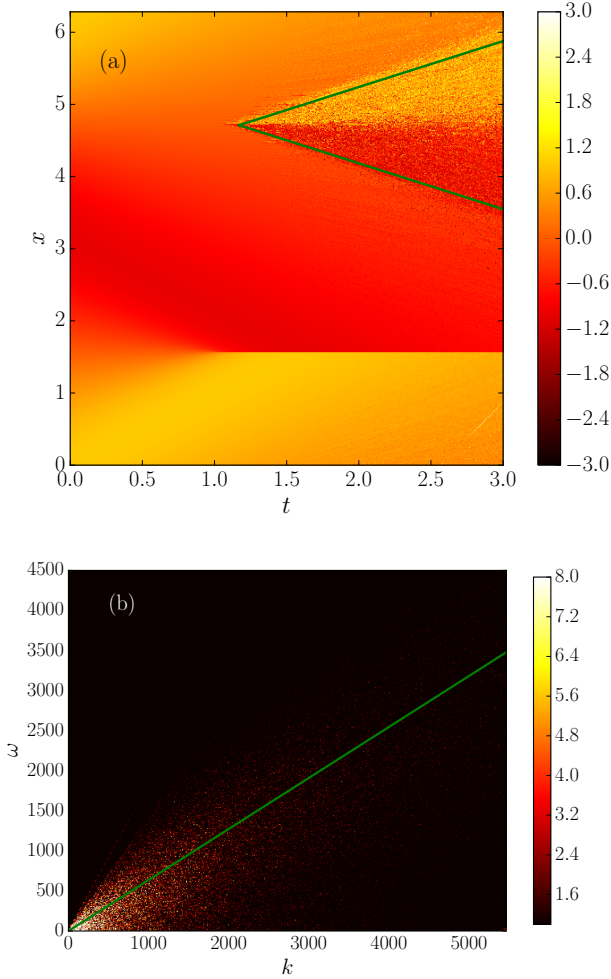


FIG. 2. (Color online) Spatiotemporal evolution of  $u(x, t)$ : (a) Evolution in real space as a function of space and time, and (b) evolution in Fourier space as a function of frequency and wave number. The spreading of the tyger after  $t = 1.1$  is well described by a velocity (marked in both plots with a green solid line) equal to  $2/\pi$ . This is the mean velocity of propagation of each thermalized subdomain formed to the right and left of the tyger when the tyger appears.

tyger appears to the time when both partially thermalized states have developed (from  $t = 1$  to  $t = 3$ ). A flat-top window function is used to correct for the fact that the signals are not periodic in time. Accumulation of energy near the relation  $\omega = Uk$  (with  $U = 2/\pi$ ), as observed in Fig. 2(b), indicates that a large number of modes propagate in real space with this velocity, confirming the observation in Fig. 2(a).

We propose the following phenomenological argument to explain the behavior of the tyger fronts during the transient from its formation to the system thermalization, and to explain their observed mean velocities. The shock and the tyger cut the total domain into two subdomains. Thermalization is then achieved first partially in these subdomains, and then eventually fully in the to-

tal domain. Each tyger front is then considered as the partially thermalized solution of each subdomain, with mean  $\mu$  and variance  $\sigma$  equal to the mean velocity and mean energy inside each subdomain. So, taking the first subdomain between  $-\pi/2$  (or  $3\pi/4$  in the periodic domain) and  $\pi/2$ , we can get the mean velocity and mean energy directly from the initial condition, namely

$$\mu = \frac{1}{\pi} \int_{-\pi/2}^{\pi/2} \cos(x) dx = \frac{2}{\pi}, \quad (9)$$

and

$$\sigma^2 + \mu^2 = \frac{1}{\pi} \int_{-\pi/2}^{\pi/2} \cos^2(x) dx = \frac{1}{2}. \quad (10)$$

Note  $\mu$  coincides with the observed velocity at which the fronts of the tygers propagate.

To test the validity of the assumption that each region is a partially thermalized solution with mean and variance set by the conservation of momentum and of energy, we compute the probability density functions (PDFs) of  $u$  at different times; these are shown in Fig. (3). For early times the system has the PDF of the cosine function, with two sharp peaks at  $u = \pm 1$  as expected. At the time of the formation of the tyger ( $t = 1.1$ ) this PDF is slightly modified; the generation of the tyger and evolution at early times was studied in detail in [15, 20, 21]. For late times ( $t = 10$ ), when the system is fully thermalized, the PDF matches that of a Gaussian with zero mean and a standard deviation of  $1/2$ , also as expected from the Gibbs ensemble [19]. But for times in between, the PDFs have two well defined peaks. To test that each tyger front is close to a partially thermalized solution with mean and standard deviation as calculated above, we plot at  $t = 3$  and  $4.1$  in Figs. 3(c) and 3(d) a bimodal distribution of the form

$$\frac{1}{2\sqrt{2\pi}\sigma^2} \left( e^{-\frac{(u-\mu)^2}{2\sigma^2}} + e^{-\frac{(u+\mu)^2}{2\sigma^2}} \right), \quad (11)$$

where the values of  $\mu$  and  $\sigma$  come from Eqs. (9). The proposed distributions are in good agreement with the data, without any free parameters to improve the adjustment. Of course, as the computation of the PDF in the simulation is done using the entire raw data and thus mixes values from the tyger fronts and from the non-thermalized parts of the solution, the match is not perfect. But in spite of this, the mean and width of the peaks are very well captured with the simple phenomenological model. Moreover, the position and width of the peaks do not change significantly during the transient, getting closer in time to the bimodal Gaussian distribution (see  $t = 4.1$ ). In the Appendix, we show the PDF of  $u$  at  $t = 3$  using different resolutions. As stated above, our results hold for all the resolutions studied. As the fronts of the tygers reach  $\pi/2$  from the left and the right of the shock, and cover the entire domain (see  $t = 7$  in Figs. 1 and 3) the two peaks suddenly merge into a PDF close

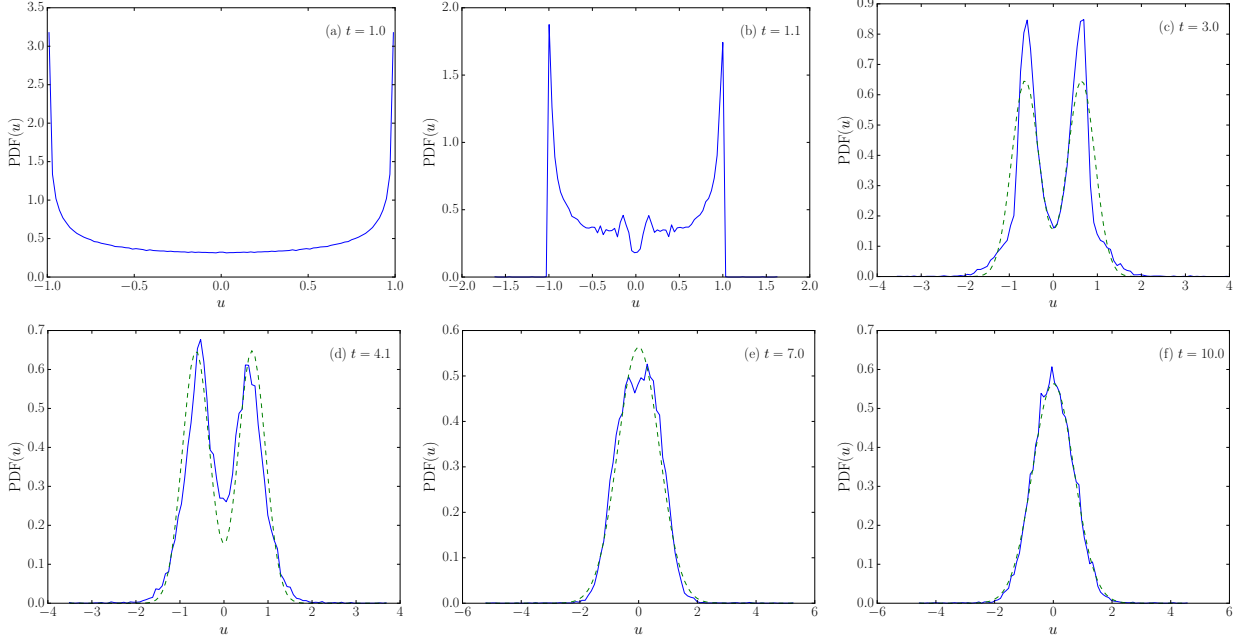


FIG. 3. (*Color online*) Probability density function (PDF) of  $u(x, t)$  at different times in (blue) solid lines; in (green) dashed lines is the proposed PDF for that instant. At the time of shock formation (a) the typical PDF of a trigonometric function can be observed, then the tyger appears at (b). At intermediate times the solution is partially thermalized and a bimodal Gaussian distribution gives a good approximation to the data, as seen in (c) and (d); the mean and standard deviation of each thermalized mode is such that the tyger front matches the statistical properties of the solution in the subdomain where it lives. At later times, (e) and (f), after the two fronts meet, the system reaches the last stages of thermalization and the solution now matches the PDF of white noise with statistical properties close to those of the thermal equilibrium. (a)  $t = 1.0$ , (b)  $t = 1.1$ , (c)  $t = 3.0$ , (d)  $t = 4.1$ , (e)  $t = 7.0$ , and (f)  $t = 10.0$ .

to Gaussian that converges to the equilibrium solution. In order to have a better understanding of how these distributions behave, we show in Fig. 4 the time evolution of the peaks of the PDFs shown in Fig. 3. These peaks are first positioned around 1 and  $-1$ , but when the partial thermalization becomes prominent we see the values of the peaks to be around  $2/\pi$  and  $-2/\pi$ . Eventually, the two tyger fronts merge and the final peak is indeed centered at zero.

As an independent test we now analyze the evolution of the system using the two-mode initial condition  $u_2(x)$  given by Eq. (7). A snapshot of  $u(x, t)$  just prior to the formation of the shocks is shown in Fig. 5(a), and another one after two tygers have formed is shown in Fig. 5(b). As this initial condition generates two shocks, one tyger is formed for each shock. The points where the shocks form are those that have  $\partial_x u < 0$  and  $\partial_{xx}^2 u = 0$ . The tygers form far away from the shocks, at the points of the solution with positive strain that move with the same velocity as each shock (note the shocks in this case move with  $u \neq 0$ ). The velocity of each shock can be obtained just by inspection of the value of  $u$  at the points where the shocks are, and the point with the same velocity but with  $\partial_x u > 0$  in Fig. 5(a) is indeed the point where each tyger appears; see also Fig. 5(b) to see the tygers after the collapse.

Following the previous argument, the tygers and the shocks separate the flow in four regions (marked in different line styles and colors in Fig. 5): one region to the left of each tyger until the nearest shock or tyger takes place, another region to the right of each tyger until the nearest shock or tyger takes place, and a region in the center of the domain bounded by two shocks. This region shows less noise, while all the other regions show signs of partial thermalization as the fronts of the tygers propagate. Figure 5(c) shows the PDF of the velocity field at  $t = 1$ . In the PDF of the data, three peaks are present. Superimposed to this PDF are shown three PDFs obtained using the same methodology as described before. The proposed PDF on the left is a Gaussian distribution with  $\mu$  and  $\sigma$  given by the mean velocity and energy of the initial conditions in the region marked by the thick (red) line (this region has mean velocity  $\mu = -1.22$  and a standard deviation of 0.24). The proposed PDF on the right is a Gaussian distribution with  $\mu$  and  $\sigma$  obtained from the initial condition in the region marked with the (green) dashed line (with mean velocity 1.48 and standard deviation of 0.39). And the proposed PDF on the middle corresponds to the region between the two tygers, which has mean velocity equal to zero; the values of  $\mu$  and  $\sigma$  of the Gaussian distribution were obtained from the initial conditions in the region indicated by the (cyan)

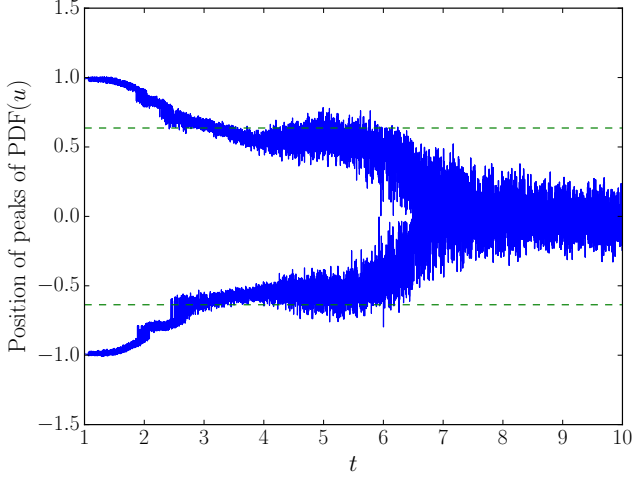


FIG. 4. (*Color online*) Evolution of the the position of the peaks of the histograms shown in Fig. 3, as a function of time. It is clear how these peaks start being wide apart and centered around 1 and -1. Then, while the behavior of the PDF is that of a bimodal Gaussian distribution, these values fluctuate around  $2/\pi$  and  $-2/\pi$  (these values are indicated by the horizontal dashed green lines), and finally they vanish as equilibrium is reached in the whole domain.

thickest line. Amplitudes of the Gaussian distributions are proportional to the area covered by each region. The two Gaussian distributions on the left and right are in good agreement with the data; the difference between the big center peak in the middle and the proposed PDF is the contribution of the region between the two fronts which is isolated from the tygers.

As an independent test and as a way to better understand the dynamics of the solution with the two-mode initial condition, we show the spatio-temporal plot of  $u(x, t)$  and the corresponding spatio-temporal spectrum in Fig. 6. The dashed blue lines correspond to the velocity of the shocks, while the solid green lines are the mean velocities of the tygers. The regions marked in cyan, green and red in Fig. 5(b), where the average is taken to calculate the mean and variance of each tyger, are the regions between the dashed and the solid lines in Fig. 6(a). The evolution of the shocks and the tygers stemming from them (as well as their mean velocities, indicated by the slopes of the straight lines) can be clearly seen.

Similar results were obtained in tests using different initial conditions that give rise to three or more shocks. The results thus confirm that each region bounded by shocks or by tygers goes through a partial thermalization, and that its properties (as well as the mean velocity at which the front of the tyger propagates) can be obtained from the available momentum and energy in the same region at  $t = 0$ . The fronts (and the tygers) act separating regions with different thermodynamical properties (i.e., with different values of  $\mu$  and  $\sigma$ ). As the shocks and the tygers propagate through the entire domain, and as the

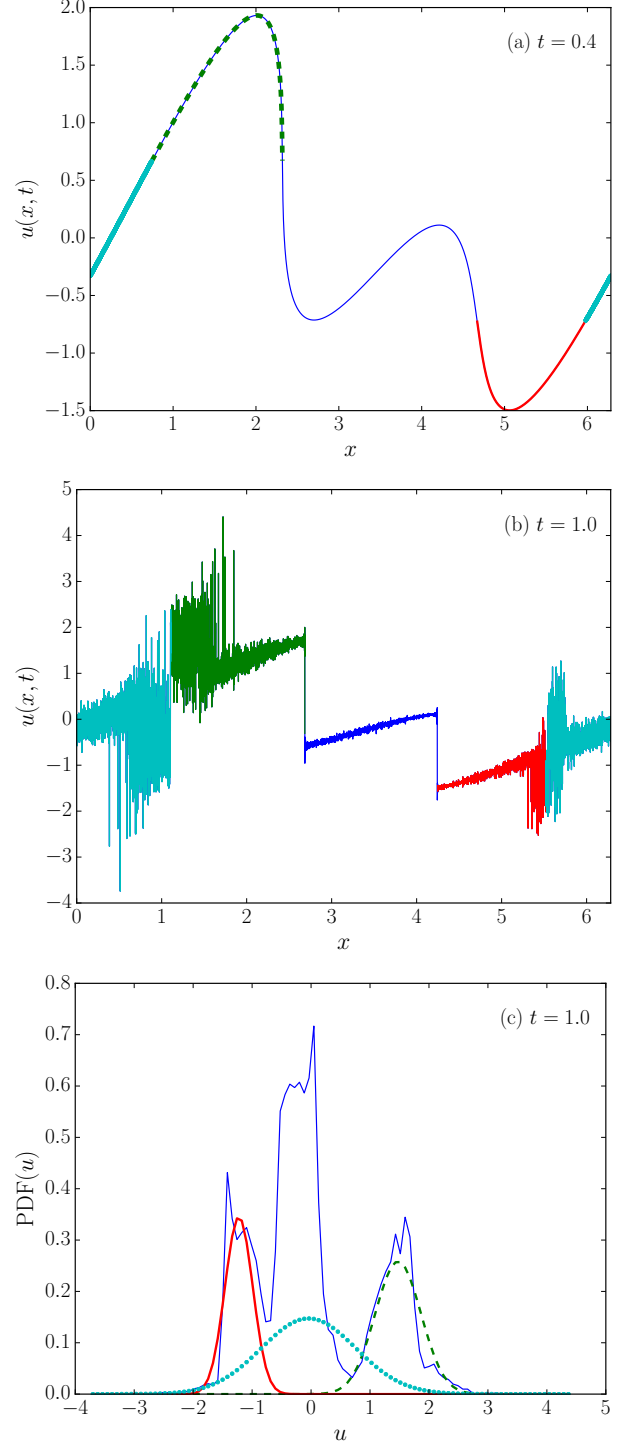


FIG. 5. (*Color online*) (a) and (b): Evolution of  $u(x, t)$  at different times in a simulation with a two-mode initial condition. Two shocks are formed now, and thus two tygers. (c): PDF of  $u(x, t = 1)$  and proposed PDF for each tyger front. The (green) dashed line in (a) marks the region (before and after the appearance of the shock) contributing to the right peak of the PDF in (c). The mean and standard deviation of this region is the same as the normal distribution plotted with (green) dashed lines in (c). The same applies to other (colored) shaded regions in all three figures.



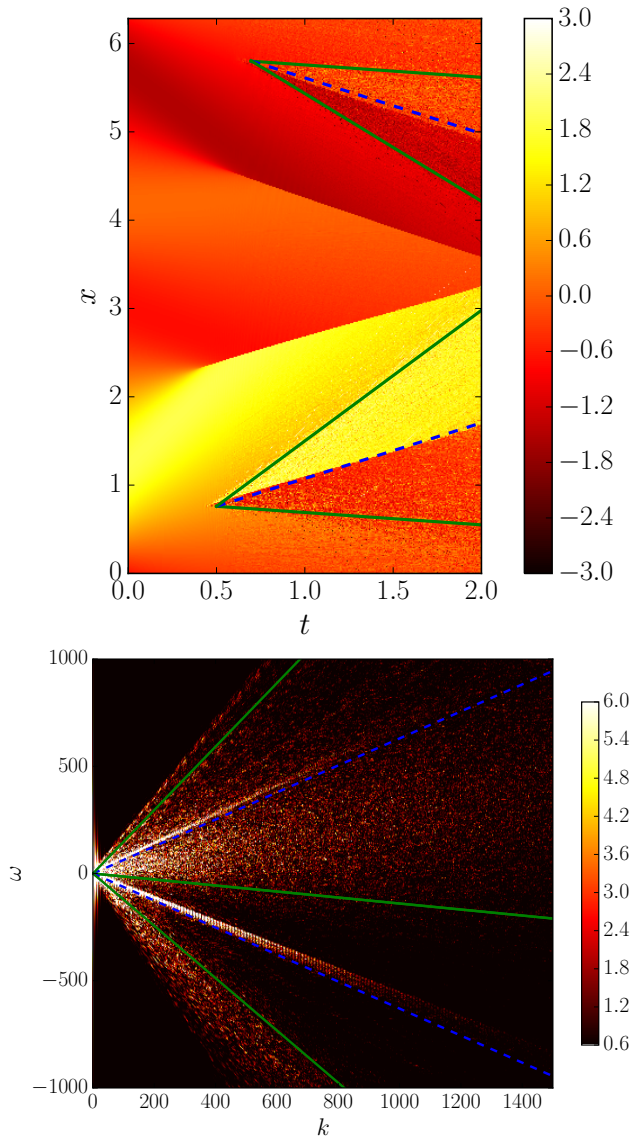


FIG. 6. (*Color online*) Spatio-temporal evolution of  $u(x, t)$  from a simulation with a two-mode initial condition: (a) Evolution in real space as a function of space and time, and (b) evolution in Fourier space as a function of frequency and wave number. The dashed (blue) lines correspond to the shock velocities, while the solid (green) lines correspond to the tygers. As two shocks form in this case, tygers appear from two different sites. The simple phenomenological theory we present is able to reproduce the mean velocity of each tyger.

fronts meet, the system finally reaches the thermalized equilibrium described by a unique Gaussian distribution function for the velocity, with a value of  $\mu$  and  $\sigma$  for the entire domain.

## V. CONCLUSIONS

The transition from deterministic solutions to stochastic thermalized equilibria in spectrally truncated hydrodynamics problems is still riddled with open questions. Its study can give new insights in problems such as the development of singularities in inviscid flows, or the development of new numerical methods for the integration of ideal equations if the growth of thermalized solutions can be controlled or removed. For the case of the Burgers equation, a simple model which still exhibits remarkably complex behavior and which is often used as a toy model of turbulence, its long-time solutions are known [19], and the triggering of the thermalization has been understood through the discovery of the so-called tygers [15].

In this work we considered the intermediate time evolution of the tygers, after their formation, and before the system reaches the thermalized regime. While in previous works (see, e.g., [5]) it was found that thermalization takes place gradually in Fourier space, here we found for the Burgers equation that in real space the two phases (thermalized and a non-thermalized) coexist with well defined regions separated by shocks and tygers. The propagation of the tygers, which take place with a well defined mean velocity, results in the growth of the partially thermalized regions until the system reaches the equilibrium solution. Moreover, the mean velocity of propagation of the fronts, as well as the thermal properties of each sub-domain, can be obtained from the conservation of the momentum and of the energy in each region.

### Appendix: Comparison of simulations with different resolutions

In Fig. 7 we show the PDF of  $u$  at  $t = 3$  for different simulations, all with the same initial condition but with different spatial resolution. In all cases we plot the same bimodal Gaussian distribution (with the same parameters  $\mu$  and  $\sigma$  coming from Eqs. (9) and (10)) as in Figs. 3(c) and (d), and in all cases it properly describes the behavior of the PDF. Aside from the more ragged looks of the lower resolution simulations, which is just the result of having less data points to construct the histograms, all simulations display the same dynamics.

## ACKNOWLEDGMENTS

The authors acknowledge financial support from Grant No. ECOS-Sud A13E01. P.C.dL. and P.D.M. acknowledge support from UBACYT Grant No. 20020130100738BA, and PICT Grants Nos. 2011-1529 and 2015-3530. P.C.dL. acknowledges funding from the European Research Council under the European Community's Seventh Framework Program, ERC Grant Agreement No. 339032.

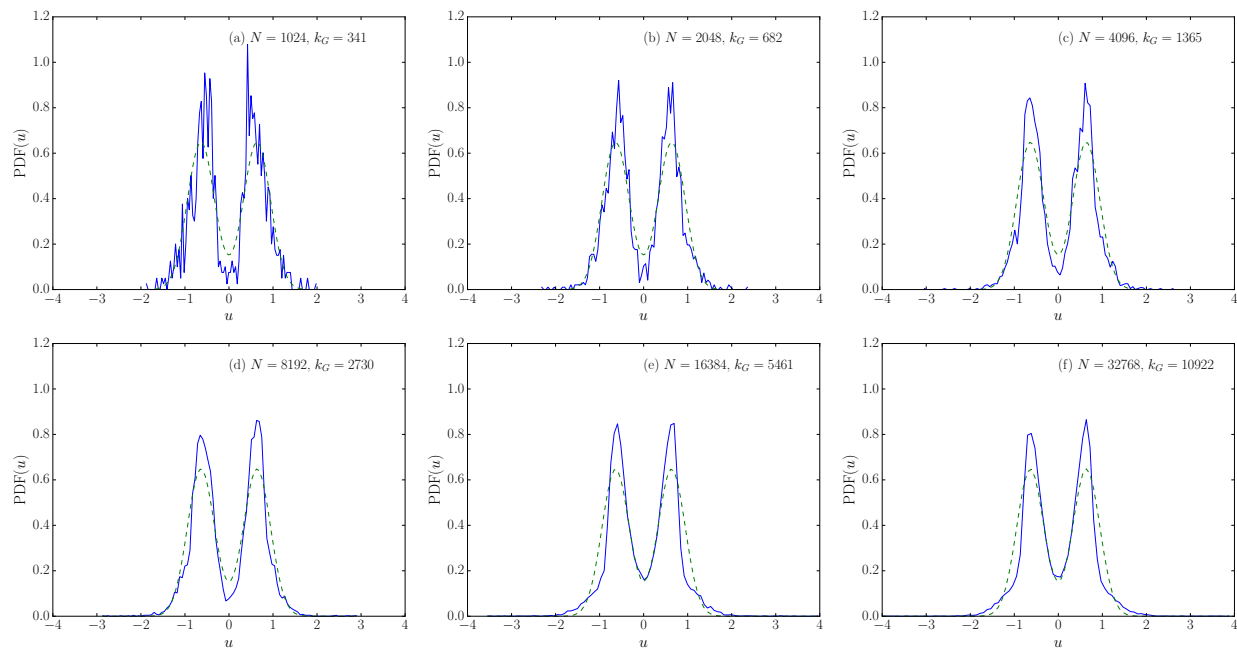


FIG. 7. (*Color online*) Probability density function (PDF) of  $u(x,t)$  at  $t = 3$  for different simulation in (blue) solid lines; in (green) dashed lines is the proposed PDF. All simulations have the same initial condition but different resolutions. The bimodal Gaussian distribution plotted is the same for every case. Our results are independent of resolution for the resolutions studied.

- 
- [1] Robert H. Kraichnan and Shiyi Chen, “Is there a statistical mechanics of turbulence?” *Physica D: Nonlinear Phenomena* **37**, 160–172 (1989).
  - [2] T. D. Lee, “On some statistical properties of hydrodynamical and magneto-hydrodynamical fields,” *Quarterly of Applied Mathematics* **10**, 69–74 (1952).
  - [3] Robert H. Kraichnan, “Inertial Ranges in Two-Dimensional Turbulence,” *Physics of Fluids* **10**, 1417–1423 (1967).
  - [4] A. C. Ting, W. H. Matthaeus, and D. Montgomery, “Turbulent relaxation processes in magnetohydrodynamics,” *Phys. Fluids* **29**, 3261 (1986).
  - [5] Cyril Cichowlas, Pauline Bonati, Fabrice Debbasch, and Marc Brachet, “Effective Dissipation and Turbulence in Spectrally Truncated Euler Flows,” *Phys. Rev. Lett.* **95**, 264502 (2005).
  - [6] G. Krstulovic, P. D. Mininni, M. E. Brachet, and A. Pouquet, “Cascades, thermalization, and eddy viscosity in helical Galerkin truncated Euler flows,” *Phys. Rev. E* **79**, 056304 (2009).
  - [7] Giorgio Krstulovic, Marc-Etienne Brachet, and Annick Pouquet, “Alfvén waves and ideal two-dimensional Galerkin truncated magnetohydrodynamics,” *Phys. Rev. E* **84**, 016410 (2011).
  - [8] Giorgio Krstulovic, Carlos Cartes, Marc Brachet, and Enrique Tirapegui, “Generation and characterization of absolute equilibrium of compressible flows,” *International Journal of Bifurcation and Chaos* **19**, 3445–3459 (2009).
  - [9] Giorgio Krstulovic and Marc Brachet, “Energy cascade with small-scale thermalization, counterflow metastability, and anomalous velocity of vortex rings in Fourier-truncated Gross-Pitaevskii equation,” *Phys. Rev. E* **83**, 066311 (2011).
  - [10] Jian-Zhou Zhu, “Isotropic polarization of compressible flows,” *J. Fluid Mech.* **787**, 440–448 (2016).
  - [11] Jian-Zhou Zhu and Gregory W. Hammett, “Gyrokinetic statistical absolute equilibrium and turbulence,” *Physics of Plasmas* **17**, 122307 (2010).
  - [12] P. Dmitruk, P. D. Mininni, A. Pouquet, S. Servidio, and W. H. Matthaeus, “Magnetic field reversals and long-time memory in conducting flows,” *Phys. Rev. E* **90**, 043010 (2014).
  - [13] Srinivasa Gopalakrishnan Ganga Prasath, Stphan Fauve, and Marc Brachet, “Dynamo action by turbulence in absolute equilibrium,” *EPL (Europhysics Letters)* **106**, 29002 (2014).
  - [14] T. Teitelbaum and P. D. Mininni, “Thermalization and free decay in surface quasigeostrophic flows,” *Phys. Rev. E* **86**, 016323 (2012).
  - [15] Samriddhi Sankar Ray, Uriel Frisch, Sergei Nazarenko, and Takeshi Matsumoto, “Resonance phenomenon for the Galerkin-truncated Burgers and Euler equations,” *Phys. Rev. E* **84**, 016301 (2011).
  - [16] Peter D. Lax and C. David Levermore, “The zero dispersion limit for the Korteweg-deVries KdV equation,” *PNAS* **76**, 3602–3606 (1979).
  - [17] Jonathan Goodman and Peter D. Lax, “On dispersive difference schemes. I,” *Comm. Pure Appl. Math.* **41**, 591–



- 613 (1988).
- [18] Thomas Y. Hou and Peter D. Lax, “Dispersive approximations in fluid dynamics,” *Comm. Pure Appl. Math.* **44**, 1–40 (1991).
  - [19] A. J. Majda and I. Timofeyev, “Remarkable statistical behavior for truncated Burgers Hopf dynamics,” *PNAS* **97**, 12413–12417 (2000).
  - [20] Divya Venkataraman and Samriddhi Sankar Ray, “The onset of thermalization in finite-dimensional equations of hydrodynamics: insights from the Burgers equation,” *Proc. R. Soc. A* **473**, 20160585 (2017).
  - [21] Peihua Feng, Jiazhong Zhang, Shengli Cao, S. V. Prants, and Yan Liu, “Thermalized solution of the Galerkin-truncated Burgers equation: From the birth of local structures to thermalization,” *Communications in Nonlinear Science and Numerical Simulation* **45**, 104–116 (2017).
  - [22] Jrmie Bec and Konstantin Khanin, “Burgers turbulence,” *Physics Reports* **447**, 1–66 (2007).
  - [23] Michele Buzzicotti, Luca Biferale, Uriel Frisch, and Samriddhi Sankar Ray, “Intermittency in fractal Fourier hydrodynamics: Lessons from the Burgers equation,” *Phys. Rev. E* **93**, 033109 (2016).
  - [24] U. Frisch, T. Matsumoto, and J. Bec, “Singularities of Euler Flow? Not Out of the Blue!” *Journal of Statistical Physics* **113**, 761–781 (2003).
  - [25] J. D. Gibbon, “The three-dimensional Euler equations: Where do we stand?” *Physica D: Nonlinear Phenomena* **237**, 1894–1904 (2008).
  - [26] P. Clark di Leoni, P. J. Cobelli, P. D. Mininni, P. Dmitruk, and W. H. Matthaeus, “Quantification of the strength of inertial waves in a rotating turbulent flow,” *Phys. Fluids* **26**, 035106 (2014).
  - [27] P. Clark di Leoni, P. D. Mininni, and M. E. Brachet, “Helicity, topology, and kelvin waves in reconnecting quantum knots,” *Phys. Rev. A* **94**, 043605 (2016).